

bbbbbb.pdf

By nfhariby@uqu.edu.sa dsr_api

Structural, optical and photocatalytic activity of Ce³⁺ doped Co–Mg nanoparticles for wastewater treatment applications

Abstract

Chemical effluent, particularly organic dyes, has become a major problem of our day because of its connection to carcinogenic health risks. Hence, rare earth element cerium (Ce) doped cobalt-magnesium ferrites were prepared with the formula $\text{Co}_{0.7}\text{Mg}_{0.3}\text{Ce}_x\text{Fe}_{2-x}\text{O}_4$ (labeled CMCF) by a combustion approach as an efficient nano-photocatalyst deliberated for disposal these pernicious dyes. The characterization tests for the CMCF nanoferrites were performed via XRD, STEM-EDS, and DR techniques. XRD results asserted the spinel single-phase formation for all the prepared CMCF ferrites. The lattice parameter and crystallite size of CMCF nanoferrites have abnormal behavior, which diminishes from 8.4077 to 8.3922 Å and 34.66 to 20.76 nm, respectively, despite the superseding process is a larger ion (Ce) instead of a smaller one (Fe). STEM images of the prepared nanoparticles are almost spherical crystallites with some agglomerations. The optical band gap of CMCF nanoparticles was tuned to be narrower by Ce³⁺ additions. Using the photocatalyst CMCF(x=0.1), the MB's hue faded from blue to nearly colorless with an efficiency of 95.49 %, in 60 min. Three reasons why the CMCF(x=0.1) photocatalyst gets the superior photocatalytic performance. Four steps were introduced to manifest the MB degradation mechanism utilizing the CMCF(x=0.1) photocatalyst. The CMCF nanomaterials have significant prospects to be operated as promising photocatalysts for toxic MB disposal through wastewater treatment processes.

1. Introduction

Toxic contaminants, such as organic dyes, are released into the environment via the disposal of industrial effluent. Besides polluting water, dyes industrial effluent slows down photosynthesis in plants and animals, causing problems in aquatic ecosystems. Many dyes are cancerous, have little biodegradability, and have a half-life of over two months under sunlight. It is thus of significant concern to the scientific world that dyes must be eliminated (Bessy et al., 2022). Especially the stable and non-biodegradable features of the methylene blue (MB) dye make them very hazardous to people and animals (Abdo et al., 2021). For preserving human and aquatic life, the appropriate removal of dye contaminants is critical. The photocatalysis technique is preferred because it is an efficient, affordable, and environmentally friendly product (Kang et al., 2021; Li et al., 2021). Photocatalysts use solar energy in oxidation and reduction processes to decompose organic compounds. Semiconductor utilization in the photocatalysis process is a fascinating topic for scientists because of its remarkable features (Kannan et al., 2020). Semiconductor spinel ferrites, as organic dye degradation photocatalysts, are gaining great attention from scientists due to their appropriate bandgap, non-toxicity, outstanding properties, and high photostability (Zhang et al., 2021). Particularly, cobalt ferrite (CoFe_2O_4), with its stability, visible light absorption capabilities, and lower band gap value, is an excellent choice for photocatalysis applications (Mmelesi et al., 2021). Also magnesium ferrite (MgFe_2O_4), with its large surface area, narrow band gap, and non-toxicity, is considered a promising adsorbent and photocatalyst (Kaur and Jeet 2022). Therefore, a ferrite system containing both CoFe_2O_4 and MgFe_2O_4 systems was chosen to produce a superior system for photocatalysis applications. The doping process is a frequently used procedure in nanoferrite materials, which includes introducing atoms or ions of desired elements to

enhance their performance or properties [Mansour et al., 2021a; Abdo and Sadeq, 2021; Ali et al., 2021]. Rare earth (RE) elements, as La, Sm, Ce, etc., are major kind of dopants with oxidation states (3+) and (4+), which directly influence the properties of ferrites via their f-electronic arrangement that confers unique physical features. Padalia et al. reported that RE elements with 3+ state is the most stable elements (Padalia et al., 2016). Meanwhile, cerium (Ce) is a striking RE element with a stable 4+ state with electronic orders $4f^0, 5d^0, 6s^0$. Irfan et al. investigated photocatalytic activity for methylene orange dye degradation utilizing Ce ions doped Co-Cd nanoferrite system, which was nearly 50% in 60 min and 98% in 180 min (Irfan et al., 2022). Meena et al. reported that the photocatalytic efficiency of manganese ferrite was enhanced by Ce doped which reached 98% for MB dye in 75 min (Meena et al., 2021). Many researchers have studied the impact of Ce^{3+} cations in enhancing the photocatalytic efficiency of various spinel systems as; copper (Nasrabadi et al., 2016) and nickel (Somanathan et al., 2019), and cobalt-nickel (Kousar et al., 2022) ferrites. Bearing these in mind, by choosing a new ferrite system, we overcame these ferrites' major limitations. Our new system is the cerium substituted cobalt-magnesium nanoferrite as a photocatalyst, with a smaller size and higher area, which is not yet reported.

Therefore, the following aspects are the main objectives of this study: (i) synthesis and characterization of Ce substituted Co-Mg nanoferrites with formula $Co_{0.7}Mn_{0.3}Ce_xFe_{2-x}O_4$ (labeled CMCF); (ii) investigating how best to incorporate cerium ions into a ferrite lattice; (iii) studying the Ce effect in tuning the band gap energy of CMCF nanoferrites; (iv) reporting the photocatalytic mechanism of CMCF in MB degradation; (v) investigation of photocatalytic efficiency of CMCF under solar simulator irradiation for MB removal for wastewater treatment.

2. Experimental Techniques

The citrate combustion approach (Al-Bassami et al., 2020) has been utilized to prepare the new nanoferrites with the formula $\text{Co}_{0.7}\text{Mg}_{0.3}\text{Ce}_x\text{Fe}_{2-x}\text{O}_4$ (CMCF) for $x = 0-0.1$; in which x steps by 0.02. The highly pure metal nitrates and citric acid were utilized and dissolved in a minimal deionized water quantity. Then were neutralized using ammonia for a pH value reaching exactly 7 (Mansour et al., 2017), and stirred by a magnetic stirrer and then heating at a temperature $t = 250$ °C. Before starting characterization procedures, all the prepared CMCF nanoferrites were ground by a gate mortar for an hour to obtain homogenous powders. The structural elucidation of CMCF nanoferrites was complemented using a powder X-ray diffractometer, Shimadzu XRD 6000, where the 2θ span within $10^\circ-80^\circ$ utilizing a radiation $\text{Cu-K}\alpha$ ($\lambda = 0.15405$ nm). FTIR spectra for all CMCF nanoferrites were performed in the frequency span of $200-4000$ cm^{-1} on a desktop FTIR model of "Bruker Tensor 27" spectrometer". The particles and shapes of the CMCF nanoferrites were defined using Carl Zeiss STEM model "Sigma 500VP microscope". At room temperature, we measured the diffuse reflectance (DR %) of all CMCF ferrite nanoparticles. The photocatalytic efficiency of CMCF nanoferrites was studied using a 350W Xenon lamp. 10mg CMCF powder, a 0.25L MB dye solution with a 5ppm concentration, was used for the photocatalytic examination.

3. Results and discussion

3.1 XRD studies

Fig. 1 embodies the indexed XRD patterns of all CMCF ferrite samples. The XRD peaks indexing and sequence match those reported in JCPDS reference cards # 00-001-1121 and # 01-088-1943 for cobalt and magnesium ferrites, respectively. Hence, we made sure of

the formation of spinel single-phase structure within all the prepared CMCF ferrites. No extra peaks for any constituents are observed, demonstrating that the crystalline spinel structure spread out over CMCF materials without other phases. The XRD peaks width varied with other Ce^{3+} content, indicating that the surface to volume ratio modifies CMCF particles (Naik and Salker, 2012). The influence of Ce^{3+} addition on the unit cell dimensions of CMCF materials can be manifested in Fig. 2, exhibiting the 2θ values shifting of (311) peaks ($2\theta_{(311)}$) for different Ce^{3+} content. This figure obviously shows the gradual increase of $2\theta_{(311)}$ from 35.4097° to 35.4468° , with progressively lattice parameter (a_{exp}) decreased from 8.4077 to 8.3922\AA . All a_{exp} values of CMCF ferrites were calculated using the d_{hkl} spacing and hkl Miller indices via the equation $a_{\text{exp}} = d_{\text{hkl}}\sqrt{h^2 + k^2 + l^2}$ (Mansour et al., 2018a) and then listed in Table 1. Undoubtedly, this result of decreasing lattice parameter is completely unexpected where our superseding process is large cations Ce^{3+} (1.02\AA) instead of smaller ones Fe^{3+} (0.64\AA). This uncommon behavior of lattice parameter can be understood for the following reasons. The larger Ce^{3+} ions endeavor to expand the CMCF lattice, but microstrains have another active role, generating a restitution role to prevent this expansion. Obviously, the produced microstrains are larger than the expansion endeavors; hence, the CMCF lattice parameter decreases gradually. Moreover, the bond dissociation energy (E_{BD}) of the Ce-O bond is 795 kJ/mol at 298 K, and the E_{BD} of the Fe-O bond is 409 kJ/mol. Therefore Ce-O is potent and short, leading to curtailment of CMCF lattice volume and their parameter (Dasent, 1982), see Fig. 2. The crystallite size (D) and internal strain (ϵ_i) of our CMCF ferrites were calculated utilizing Williamson-Hall (W-H) approach by analyzing the XRD peak broadening by the following equation (Mansour et al., 2020).

$$\beta \cos \theta = \frac{k\lambda}{D} + 4\varepsilon_i \sin \theta$$

All W-H plots ($\beta \cos \theta$ versus $4 \sin \theta$) are manifested in Fig. 3a-f. From W-H plots, D and ε_i values are calculated from $D = (k\lambda / \text{intercepts})$ and $\varepsilon_i = \text{slope}$ of the fitted lines, where k is a constant (0.9) and λ is X-ray wavelength. All D and ε_i values are collected in Table 1, demonstrating that D values are in the nanometric range, which diminishes gradually from 34.66 to 20.76 nm with Ce/Fe superseding process. As mentioned above, this is a logical result for the EBD values disparity of Ce-O, and Fe-O bonds. Therefore more energy is requisite to force Ce^{3+} ions merge into the CMCF lattice and produce $\text{Ce}^{3+}-\text{O}^{2-}$ bonds. Consequently, our superseding process (Ce/Fe) results interior lattice stress, which prevents CMCF lattice growth and decreases their size. Hence, CMCF nanoferrites have higher thermal stability than the pristine $\text{Co}_{0.7}\text{Mg}_{0.3}\text{Fe}_2\text{O}_4$ sample where extra energy is requisite for crystallization process (Thankachan et al., 2013). Mansour et al. reported a similar result for decreasing crystallite size by doping larger ions lanthanum at the expense of iron ions (Mansour et al., 2021b). All ε_i values are positive, demonstrating that the CMCF nanoferrites have tensile strain (Mansour et al., 2019), which is a logical result for Ce/Fe superseding process.

Additional calculations were made to determine the X-ray density (d_{XRD}) (Mansour et al., 2018b) through the equation $d_{\text{XRD}} = \frac{ZM}{a^3 N_A}$, where Z is the number of molecules per unit cell, M is the molecular weight of the sample (g/mole), N_A is the Avogadro's number (6.023×10^{23} atom/mole). The specific surface area of all the samples was determined by the formula $S = \frac{6000}{D \times d_{\text{XRD}}}$ (Chahar et al., 2021). All these parameters were tabulated in Table 1.

An increasing trend for d_{XRD} values is obtained, which is a logical result for the superseding

process of Ce/Fe cations, where Ce has a molecular weight of 140.116 g/mol, and Fe has 55.85 g/mol. With additional Ce³⁺ content, S values exhibit an increment behavior, a natural conclusion of the decrementing behavior for crystallite size; See Table 1. Therefore our CMCF nanoferrites are more appropriate for providing a large surface area which is most required for absorption in photocatalysis applications, as seen later.

3.2 Electron microscopy analysis:

Fig. 4a-f shows the STEM-EDX images of Co_{0.7}Mg_{0.3}Ce_xFe_{2-x}O₄, (x= 0.0, 0.04 and 0.1) samples; as models for all CMCF nanoferrites. Fig. 4a-c manifests the STEM images for the selected samples, which confirm the nanocrystalline nature of the CMCF nanoparticles (Abdo, El-Daly, 2021). These nanoparticles are almost spherical crystallites with some agglomerations produced from the magnetic properties of the CMCF ferrites and their surface binding forces. To scrutinize the CMCF nanoparticle constituents' cations, EDX micrographs are collected for the elected nanoferrites. Fig. 4d-f shows the EDX charts of Co_{0.7}Mg_{0.3}Ce_xFe_{2-x}O₄, (x= 0.0, 0.04 and 0.08). The EDX micrographs revealed the entity of all CMCF constituents' ions only; Co, Mg, Ce, Fe, and O; confirming that our samples are pure CMCF powders without any unknown elements. These figures also show the increment of Ce quantity on account of Fe ones is nearly identical to Ce/ (Ce+Fe) percentage through the preparation process. The ratios (Co+Mg)/Fe in the pristine sample, and (Co+Mg)/ (Ce+Fe), in nanoferrites containing Ce³⁺ ions, are almost 0.5, demonstrating the CMCF nanoferrites' pureness.

3.4 Optical studies

3.4.1 DR spectroscopy of CMCF nanoferrites and their optical energy gap

Diffuse reflectance spectroscopy is used to assess the optical characteristics of the studied CMCF nanoferrites. The reflectance function (F(R)) of a suitably thick layer may be estimated utilizing Kubelka and Munk (K-M) model (Alahmari et al., 2022).

$$F(R) = \frac{(1 - R)^2}{2R}$$

The CMCF nanoferrites' energy band gap (E_g) values may well be estimated using Tauc's equation (Alahmari et al., 2022) as follows:

$$[F(R_\infty) \cdot h\nu]^{\frac{1}{n}} = A(h\nu - E_g)$$

The exponent n specifies the transition kind, **whether** direct ($\frac{1}{2}$) or indirect (2) allowed kinds. It is clear from Fig. 5a-f that the direct band gaps in our CCZY nanoferrites are applicable. When Tauc's plots converge at $y=0$, E_g will be accurately calculated in the eV unit. It is shown in Table 1 that the CMCF nanoferrites have an outstanding E_g demeanor. A sample with $x=0.0$ has an E_g value of 1.55 eV. By increasing the Ce^{3+} concentration from $x=0.02$ to $x=0.1$, the CMCF nanoferrites had lower E_g values of 1.54, 1.57, 1.54, 1.55, and 1.53 eV. Because of this, the $Co_{0.7}Mg_{0.3}Fe_2O_4$ band gap may be tuned to be ideal candidates for proper activities that fall within the semiconductor band gap range. The inverse correlation **between** E_g and crystallite size (Mansour et al., 2021c) justifies the behavior of E_g , which is based on the behavior of crystallite size. As far as we **know**, this study was the first to **investigate** the optical band gaps of $Co_{0.7}Mg_{0.3}Ce_xFe_{2-x}O_4$ nanoparticles.

3.4.2 Photocatalytic analyses

The photodegradation procedure employing nanoferrites is an **attractive** way to erode organic dyes into secure yields, H_2O and CO_2 , by sunlight (Li et al., 2022). The bandgap of our CMCF nanoparticles reduces slowly by cerium ions addition, revealing that our

nanoparticles may be operated like usable visible-light-driven efficient photocatalyst. Accordingly, the catalytic analysis of our CMCF nanoferrites is evaluated concerning a toxic organic dye, methylene blue (MB). The significance of such analysis is probing the CMCF nanoferrites utilization in wastewater treatment. The importance of operating the CMCF nanoferrites, like whole spinel nanoferrites, is long-lasting, reused several periods, have a lower expense and have a thinner bandgap. Many new results (Shakil et al., 2022; Vinosha et al., 2022) appraised efficacious outcomes for photocatalytic processes based on the RE element, nanoferrite band gap values besides their nanometric size. It is attended that the CMCF(x=0.1) nanoferrite acquires the most increased photocatalytic efficiency based on their highest Ce³⁺ ions, miniature E_g, and teeny dimension values. So, this nanoferrite is expected to produce a remarkable result for MB degradation. Some CMCF nanoferrites are preferred to probe their photocatalytic response using MB; the nanoferrite with x=0.0 (pure specimen), x=0.04 (with the moderate value of Ce³⁺ and highest E_g), and x=0.1 (highest Ce³⁺ value, lower E_g and lower size values). A solar simulator instrument was utilized to irradiate pure MB dye, and our chosen CMCF nanoferrites via a Xenon arc lamp 350 W. MB solution (0.25 L and 5 ppm) was employed with 10mg from CMCF samples for the degradation examination. Fig. 6a-d manifests the absorption graphs of pure MB, MB+CMCF(x=0.0), MB+CMCF(x=0.04) and MB+CMCF(x=0.1) collected regularly with time at (0, 10, 20, 30, 40, 50 and 60 min). In all the curves, there is a peak of nearly 600 nm with a 563 nm shoulder, indicating the MB presence. There are no red or blue shifts in our solution's photocatalytic chemical processes as the exposure duration increases from t = 0 to 60 minutes. This situation implies that our solutions contain only pure photocatalytic chemical reactions. After exposure to the light for 60 minutes, the MB's hue faded from blue

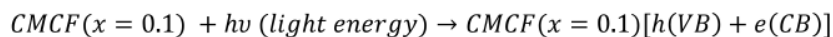
to colorless. The equivalent formula in Ref. (Zheng et al., 2022) has been used to assess the samples' degradation efficacy. Indeed, the sample CMCF(x=0.1) had the maximum degrading efficiency in MB, with a 95.49 % degradation rate after 60 minutes of exposure. This is a noteworthy finding compared with the reminder specimens; 8.21 % for solely MB, 26.73 % for CMCF(x=0.0) and 74.94 % for CMCF(x=0.04). Apparently, Fig. 7a demonstrates the photodegradation efficiency for pure MB and MB employing CMCF(x=0.0), CMCF (0.04) and CMCF (0.1) samples (as catalyst). Hence, our CMCF powders have been shown to improve MB degrading efficiency. It was reported that MB dye has a maximum degradation efficiency of 80% after 240 min utilizing a cobalt magnesium ferrite system (Dojcinovic et al., 2021). Also, another research group declared that MB dye acquired a maximum efficiency of 77 % after 60 min via a cobalt zinc ferrite system (Deepika et al., 2021). Geetha et al. declared degradation efficiency for MB utilizing Ce substituted magnesium nanoferrites ($\text{MgCe}_{0.1}\text{Fe}_{1.9}\text{O}_4$) to be 82.69 % in 90 min (Geetha et al., 2021). Consequently, the degradation efficiency of the CMCF(x=0.1) sample is an outstanding outcome (95.49 % at 60 min) compared with the literature review for MB removals. The reasons behind the sample CMCF(x=0.1) having the maximum efficiency are represented as follows:

1. It has a smaller size, 20.76 nm, and hence has a larger surface area, see Table 1, which is preferable for the catalysis process.
2. It has a lower E_g value, 1.53 eV, and thus enhances the excitations of electrons from the valence band (VB) into the conduction band (CB).
3. Cerium ions can operate as an electronic trapping center as a reminder of rare earth elements, which may slow the rate of e-h recombination.

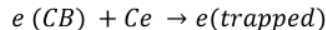
3.4.3 Degradation Mechanism

Based on the semiconductor photocatalysis concept, rare earth ferrite valence electrons are driven by 350-750 nm irradiation light to create a very active light hole-electron pair that increases its visible-light catalytic performance. The nanoferrite CMCF(x=0.1) will utilize, as a model, to discuss the MB degradation mechanism. The likely photodegradation pathway for MB employing the CMCF(x=0.1) nanoferrite is illustrated in Fig. 6e, which can summarize the following steps. Abdo et al reported a similar mechanism for MB dye degradation (Abdo et al. 2021).

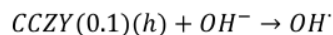
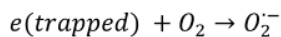
Step 1: The CMCF(x=0.1) nanoferrite absorbs the incoming energy (hv), happens electrons (e) excitation from CMCF(x=0.1) VB to their CB while departing holes (h) inside this VB.



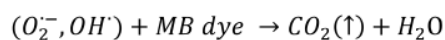
Step 2: Cerium ions work as electron capturing centers that capture the excited electrons leading to hindrance to the e-h pair combination.



Step 3: These electrons (trapped) transported from cerium ions combine with O₂ and generate superoxide radical (O₂⁻). While, h, generated in the VB of CMCF(x=0.1), can get combined with (OH⁻) to create hydroxyl radical (OH[·]).



Step 4: The produced free radicals (O₂⁻ and OH[·]) led to MB degradation into natural and harmless components (CO₂(↑) + H₂O) (Kumar and Chand, 2022).



3.4.4 The CMCF Photocatalysts Recyclability

Nanoferrites recyclability is of major **significance** because of its ability to degrade the contaminants released by dyeing pollution. An external magnet can readily extract ferrites from the reaction mixture. After 60 min, the powders were detached and dried at RT. The recovered powders were transported to a quartz cuvette with fresh MB solution for the next cycle. This process was performed in 5 runs under **similar** conditions. The stability of the as-synthesized CMCF photocatalysts is that they did not exhibit any appreciable loss even after five cycles. The MB degradation in the presence of the nanoferrite CMCF(x=0.1) for 5 subsequent cycles is represented in [Fig. 7b](#), which shows no significant loss after these cycles. From [Fig. 12](#), the MB degradation efficiencies are 95.49%, 95.34%, 95.13%, 94.97%, and 94.75%, respectively, with our CMCF photocatalyst, demonstrating their application in dye degradation and wastewater treatment.

3.4.5 Reaction kinetic studies

To identify the catalytic activity behavior of our CMCF nanoferrites, the three kinetic orders (0th, 1st and 2nd) were computed by the following relations ([Aref et al., 2020](#)).

$$A_t = A_o - k_o t, A_t = A_o e^{-k_1 t}, \frac{1}{A_t} = \frac{1}{A_o} + k_2 t$$

Wherein A_t and A_o represent absorbance after and before light irradiation. [Figs. 8a-c](#) manifest the A_t , $\ln(A_o/A_t)$ and $1/A_t$ versus time graphs for pure MB and (MB+ CMCF nanoferrites (x=0.0, 0.04, and 0.1)). The k_o , k_1 , and k_2 represent the three kinetic rate constants of 0th, 1st, and 2nd kinetics of MB and (MB+ CMCF nanoferrites (x=0.0 and 0.1) are determined then listed in [Table 2](#). [Table 2](#) also includes correlation coefficients (R^2) for each case. For all the samples pure MB and (MB+ CMCF nanoferrites (x=0.0, 0.04 and 0.1),

the zero-order is very convenient for the catalytic behavior, where its R^2 values are equal to 0.970, 0.975, 0.984 and 0.996 respectively, which are the maximum among all models.

Conclusion:

A facile, citrate combustion approach was utilized to prepare a new nanoferrite system of $\text{Co}_{0.7}\text{Mn}_{0.3}\text{Ce}_x\text{Fe}_{2-x}\text{O}_4$ (CMCF); $x=0.0-0.1$. XRD results demonstrated the formation of spinel single-phase structure within all the prepared CMCF ferrites, with no extra peaks for any constituents. Crystallite size values of all CMCF nanoferrites are in the nanometric range with decreasing behavior from 34.66 to 20.76 nm. All lattice strain values are positive, demonstrating that the CMCF nanoferrites have tensile strain. FTIR transmittance spectra of the CMCF ferrite powders revealed their distinct functional groups of tetrahedral and octahedral coordination. The EDX micrographs revealed the entity of all CMCF constituents' ions only; Co, Mg, Ce, Fe, and O, confirming the purity of our powders. The bandgap of all CMCF nanoferrites was tuned by Ce^{3+} additions and fell within the semiconductor bandgap range. The nanoferrite CMCF($x=0.1$) had the maximum degrading efficiency in MB, with a 95.49 % degradation rate after 60 minutes compared with the reminder specimens; 8.21 % for solely MB, 26.73 % for CMCF($x=0.0$) and 74.94 % for CMCF($x=0.04$). The likely photodegradation pathway for MB employing the CMCF($x=0.1$) nanoferrite may be grasped through four steps. The MB degradation using the nanoferrite CMCF($x=0.1$) after 5 subsequent cycles showed no significant. The zero-order model is the most convenient one for identifying photocatalytic behavior. The nanoferrite $\text{Co}_{0.7}\text{Mg}_{0.3}\text{Ce}_{0.1}\text{Fe}_{1.9}\text{O}_4$ can be utilized as a photocatalyst for MB effluents removal with an efficiency of 95.49% in just an hour.

2%

SIMILARITY INDEX

PRIMARY SOURCES

- 1 S.F. Mansour, M.A. Abdo, F.L. Kzar. "Effect of Cr dopant on the structural, magnetic and dielectric properties of Cu-Zn nanoferrites", Journal of Magnetism and Magnetic Materials, 2018
Crossref 21 words — 1%
- 2 pubs.rsc.org
Internet 14 words — < 1%
- 3 dyuthi.cusat.ac.in
Internet 11 words — < 1%
- 4 assets.researchsquare.com
Internet 9 words — < 1%
- 5 A.M. Dumitrescu, G. Lisa, A.R. Iordan, F. Tudorache et al. "Ni ferrite highly organized as humidity sensors", Materials Chemistry and Physics, 2015
Crossref 7 words — < 1%

EXCLUDE QUOTES OFF

EXCLUDE SOURCES OFF

EXCLUDE BIBLIOGRAPHY OFF

EXCLUDE MATCHES OFF